NAWCWPNS TP 8355

Coupling of Gaussian Incident Beam Energy into Planar Guided Wave Structures

by
J. Merle Elson and Phuc Tran
Research & Technology Group

April 1997

NAVAL AIR WARFARE CENTER WEAPONS DIVISION
CHINA LAKE, CA 93555-6100

Naval Air Warfare Center Weapons Division

FOREWORD

This work was supported by the Naval Air Warfare Center Weapons Division, China Lake In-House Labroatory Independent Research discretionary funding for fiscal year 1996.

This report was reviewed for technical accuracy by Daniel T. Gillespie

Approved by
R. L. DERR, *Head*
Research & Technology Group
15 April 1997

Under authority of
J. V. CHENEVEY
RADM, U.S. Navy
Commander

Released for publication by
S. HAALAND
Director for Research and Engineering

NAWCWPNS Technical Publication 8355

Published by . . . . . Technical Information Division
Collation . . . . . Cover, 6 leaves
First printing . . . . . 33 copies

REPORT DOCUMENTATION PAGE

Form Approved
OMB No. 0704-0188

1. AGENCY USE ONLY *(Leave blank)*	2. REPORT DATE	3. REPORT TYPE AND DATES COVERED
	April 1997	Interim report - October 1996—September 1997

4. TITLE AND SUBTITLE
Coupling Of Gaussian Incident Beam Energy Into Planar Guided Wave Structures

5. FUNDING NUMBERS
N0001496WX20167

6. AUTHOR(S)
J. Merle Elson and Phuc Tran

7. PERFORMING ORGANIZATION NAME(S) AND ADDRESS(ES)
Naval Air Warfare Center Weapons Division
China Lake, CA 93555-6100

8. PERFORMING ORGANIZATION REPORT NUMBER
NAWCWPNS TP 8355

9. SPONSORING/MONITORING AGENCY NAME(S) AND ADDRESS(ES)
Office of Naval Research
ONR 354-Dr. Ronald Kostoff
Ballston Tower One
800 N. Quincy St.
Arlington, VA 22217-5660

10. SPONSORING/MONITORING AGENCY REPORT NUMBER

11. SUPPLEMENTARY NOTES

12A. DISTRIBUTION/AVAILABILITY STATEMENT
A Statement; distribution unlimited

12B. DISTRIBUTION CODE

13. ABSTRACT *(Maximum 200 words)*

(U) A two-dimensional, finite-difference, coupled-mode method is applied to calculate endwise coupling of Gaussian beams into planar waveguides. Polarization with the electric or magnetic vector parallel to the waveguide boundaries is considered. Numerical results indicate that, for the model waveguide considered, most of the Gaussian energy is coupled into the waveguide. For polarization with the magnetic vector parallel to the waveguide boundary, the incident beam couples with evanescent surface modes and propagating modes.

14. SUBJECT TERMS
Gaussian Beam
Waveguide Coupling
Electromagnetic Theory

15. NUMBER OF PAGES
11

16. PRICE CODE

17. SECURITY CLASSIFICATION OF REPORT	18. SECURITY CLASSIFICATION OF THIS PAGE	19. SECURITY CLASSIFICATION OF ABSTRACT	20. LIMITATION OF ABSTRACT
UNCLASSIFIED	UNCLASSIFIED	UNCLASSIFIED	UL

INTRODUCTION

We consider the case of a monochromatic cylindrical beam with Gaussian intensity profile, which is incident endwise upon a semi-infinite planar waveguide structure. This study can have practical implications for electro-optic devices where coupling of laser energy into guided wave devices is of interest.

Shown schematically in Figure 1, the Gaussian beam is incident at angle θ onto the $z = 0$ plane where this plane defines the boundary between the superstrate and substrate. The problem analyzed here is two-dimensional, where the incident beam and waveguide structure are invariant in the y dimension.

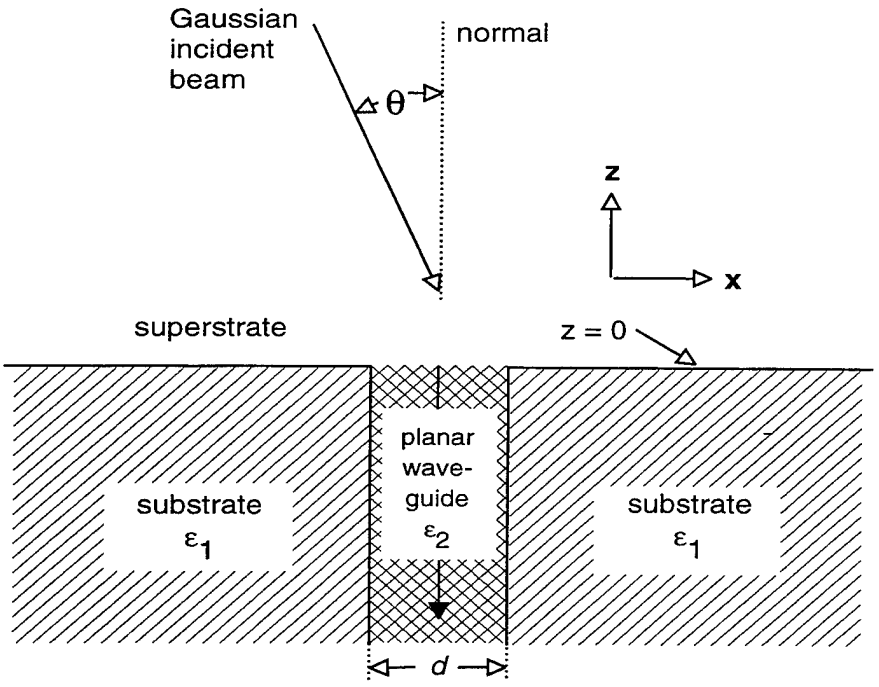

FIGURE 1. Schematic of a Gaussian Beam Incident Endwise Upon a Semi-Infinite Planar Waveguide. The Gaussian beam and waveguide channel are invariant in the y-direction. The shaded substrate regions with permittivity ε_1 border the planar waveguide channel which has permittivity ε_2. The substrate regions are semi-infinite in the $\pm x$ directions and the waveguide has width d. Also, the substrate and waveguide are both semi-infinite in the $-z$ direction.

METHOD OF COMPUTATION

The plane $z = 0$ separates two semi-infinite media. The superstrate region $z \geq 0$ is homogeneous and the substrate region, which is invariant in the $-z$ direction, contains a planar waveguide structure of width d. We assume a monochromatic Gaussian intensity profile beam, characterized by width σ and wavelength λ, is normally incident on the waveguide structure. We approximate the amplitude of the Gaussian beam at $z = 0$ by

$$P_y^{inc}(x, z = 0) = \exp\left[-x^2 / \sigma^2\right] \tag{1}$$

where P_y^{inc} represents the y component of either the electric or magnetic field, whichever is appropriate. When the (electric) magnetic field is parallel to the waveguide boundaries, P_y^{inc} is the (electric) magnetic field amplitude. We wish to calculate the transmitted and reflected fields where we expect at least part of the transmitted energy to be in the form of a guided wave.

The approach used in this work has similarities to previous work (References 1 through 5). In References 1 through 3, solutions were obtained as modal expansions similar to that done here. In Reference 1, the solution was obtained entirely in Fourier space and digitization of real space is not done. In References 2 through 3, real space is discretized as is done in the present work. In Reference 4 and also in real space, a numerical integration of Maxwell's equations is done without the need for modal expansion solutions. Finally, in Reference 5, the present method was applied to investigate transverse localization of electromagnetic propagation in alternating high-low dielectric media of random thickness. Like the work here, the incident beam was Gaussian and incident endwise on the laminate structure.

Along the x direction, a discrete set of n_x points, separated by Δx, is defined that are symmetrically located about $x = 0$. This is shown in Figure 2. The total width of these points is $L = n_x \Delta x$ and this defines the lateral limits ($x = \pm L/2$) of the calculation region along the x direction. Because of this, we require that $L >> \sigma$ so that the incident field is essentially zero at the limits $x = \pm L/2$. No attempt is made to incorporate transparent boundary conditions at the lateral limits of the calculation region. The field at the lateral limit and beyond is always assumed to be zero. If nonzero field intensity reaches the lateral limit boundary, for whatever reason, then the calculation is terminated. A simple example is when the substrate region is a homogeneous dielectric material (no waveguide channel). In this case, the width of the transmitted field, relative to the initial Gaussian width, would spread out with increasing depth by means of diffraction and eventually reach the lateral limit boundary. In this case, the field would probably "reflect" from the boundary, and this would be nonphysical since the boundary is fictitious.

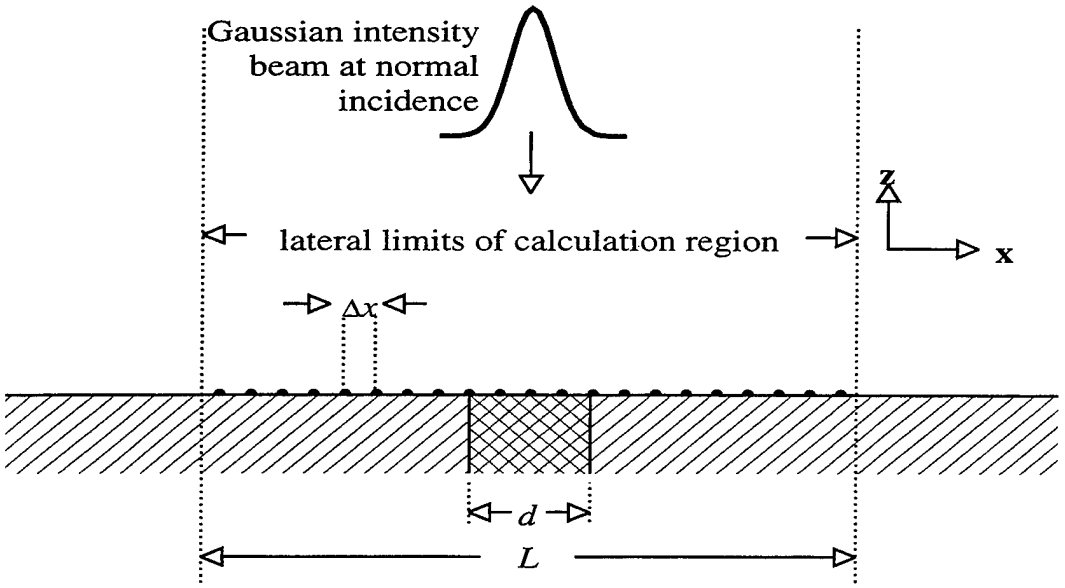

FIGURE 2. Schematic Illustrating x Coordinate Discretization (Solid Dots Separated by Δx) With x-Limits on Extent of Calculation Region (Shown by Length L Between the Vertical Dotted Lines). The incident field is negligible at the extreme limits. In this example the solid dots represent n_z=21 digitized x coordinates.

Solutions to Maxwell's equations in the homogeneous $z > 0$ region are straightforward and not discussed here. In the inhomogeneous $z \leq 0$ region, the solutions are more complicated and with the x coordinate digitized, we write the x dependence of the two Maxwell's equations $\nabla \times \mathbf{E}(\mathbf{r}) = i(\omega/c)\mathbf{B}(\mathbf{r})$ and $\nabla \times \mathbf{B}(\mathbf{r}) = -i(\omega/c)\mathbf{D}(\mathbf{r})$, where $\mathbf{D}(\mathbf{r}) = \varepsilon(\mathbf{r})\mathbf{E}(\mathbf{r})$, in centered finite-difference form. In the $z \leq 0$ region, this yields:

$$\frac{\partial E_x(x,z)}{\partial z} = \frac{i\omega}{c} B_y(x,z) + \frac{ic}{\omega(\Delta x)^2}\left\{\frac{B_y(x+\Delta x,z) - B_y(x,z)}{\varepsilon(x+\Delta x/2)} + \frac{B_y(x-\Delta x,z) - B_y(x,z)}{\varepsilon(x-\Delta x/2)}\right\} \tag{2a}$$

$$\frac{\partial E_y(x,z)}{\partial z} = -\frac{i\omega}{c} B_x(x,z) \tag{2b}$$

$$\frac{\partial H_x(x,z)}{\partial z} = -\frac{i\omega}{c}\varepsilon(x)E_y(x,z)$$

$$+\frac{ic}{\omega(\Delta x)^2}\left\{2E_y(x,z) - E_y(x+\Delta x,z) - E_y(x-\Delta x,z)\right\} \tag{2c}$$

$$\frac{\partial H_y(x,z)}{\partial z} = \frac{i\omega}{c}\varepsilon(x)E_x(x,z) \tag{2d}$$

where the z coordinate remains a continuous variable. The z components of the fields have been eliminated since the $z \leq 0$ region is invariant along the z direction. The permittivity $\varepsilon(x)$ describes the substrate region where $\varepsilon(x) = \varepsilon_1$ when $|x| > d/2$ and $\varepsilon(x) = \varepsilon_2$ when $|x| \leq d/2$. Equation 2 is versatile since the only part that depends on the waveguide structure is the permittivity $\varepsilon(x)$, and this quantity can be configured to represent a variety of situations. Equation 2 is valid at a discrete point x in the set of n_x points and since we must collectively consider all of the x points, this results in a coupled equation system totaling $4n_x$ equations. The equations associated with all n_x points which cover distance $L = n_x\Delta x$ may be concisely written in matrix form as

$$\frac{\partial \mathbf{A}(\mathbf{X},z)}{\partial z} = \mathbf{M}(\mathbf{X})\mathbf{A}(\mathbf{X},z) \tag{3a}$$

where

$$\mathbf{A}(\mathbf{X},z) = \begin{pmatrix} E_x(\mathbf{X},z) \\ E_y(\mathbf{X},z) \\ B_x(\mathbf{X},z) \\ B_y(\mathbf{X},z) \end{pmatrix} \tag{3b}$$

Since $\mathbf{M}(\mathbf{X})$ is independent of z, the solution for the fields in the $z \leq 0$ region is straightforward by diagonalization of $\mathbf{M}(\mathbf{X})$:

$$\mathbf{A}(\mathbf{X},z) = \mathbf{S}(\mathbf{X})\mathbf{exp}(\Lambda z)\mathbf{C} = \begin{pmatrix} \mathbf{S}_{11} & \mathbf{S}_{12} \\ \mathbf{S}_{21} & \mathbf{S}_{22} \end{pmatrix}\begin{pmatrix} \mathbf{e}^{\lambda z} & \mathbf{0} \\ \mathbf{0} & \mathbf{e}^{-\lambda z} \end{pmatrix}\begin{pmatrix} \mathbf{C}_+ \\ \mathbf{C}_- \end{pmatrix} \tag{4}$$

The square matrix $\mathbf{S}(\mathbf{X})$ has columns which are the eigenvectors of $\mathbf{M}(\mathbf{X})$, $\mathbf{exp}(\Lambda z)$ is a diagonal matrix with Λ representing the set of eigenvalues associated with $\mathbf{M}(\mathbf{X})$, and $\mathbf{C}$ is a column vector of constants. In the right hand side of this equation, the $\mathbf{S}$ and $\mathbf{exp}$ matrices have been sectored. The $\mathbf{exp}$ matrix has exponential terms along the diagonal where the set of eigenvalues Λ consists of pairs such that for every eigenvalue $+\lambda$, there is another eigenvalue which is equal but opposite in sign, i.e. $-\lambda$. The eigenvalue pairs $+\lambda$ and $-\lambda$ are associated with solutions that propagate or decay exponentially in the $-z$ and $+z$ directions, respectively. With this in mind, it is clear in Equation 4 that the $\mathbf{exp}$ matrix has been sectored by separating the solutions, which propagate into the $\pm z$ directions. For the problem considered in this work, solutions in the $z \le 0$ region having coefficient $\mathbf{C}_-$ are unphysical since they represent propagation in the $+z$ direction or exponentially increasing behavior as $z \to -\infty$. Because of this we set $\mathbf{C}_- = 0$ and the $z \le 0$ solution may now be written

$$\begin{pmatrix} \tilde{\mathbf{E}}^t(\mathbf{X},z) \\ \tilde{\mathbf{B}}^t(\mathbf{X},z) \end{pmatrix} = \begin{pmatrix} \mathbf{S}_{11}(\mathbf{X})\mathbf{e}^{\lambda z}\mathbf{C}_+ \\ \mathbf{S}_{21}(\mathbf{X})\mathbf{e}^{\lambda z}\mathbf{C}_+ \end{pmatrix} \tag{5}$$

where we have introduced the superscript t to denote transmitted field and the *tilde* notation to denote an abbreviated column vector as

$$\tilde{\mathbf{E}} = \begin{pmatrix} E_x \\ E_y \end{pmatrix} \quad \text{and} \quad \tilde{\mathbf{B}} = \begin{pmatrix} B_x \\ B_y \end{pmatrix} \tag{6}$$

From Equation 5 we easily relate the magnetic and electric fields in the $z \le 0$ region as

$$\tilde{\mathbf{B}}^t(\mathbf{X},z) = \mathbf{S}_{21}(\mathbf{X})\left[\mathbf{S}_{11}(\mathbf{X})\right]^{-1}\tilde{\mathbf{E}}^t(\mathbf{X},z) \tag{7}$$

We now apply the boundary conditions at the $z = 0$ boundary with the requirement that the tangential components of the electric and magnetic fields be continuous across this boundary. These conditions can be written as $\tilde{\mathbf{E}}^{inc}(\mathbf{X},0) + \tilde{\mathbf{E}}^r(\mathbf{X},0) = \tilde{\mathbf{E}}^t(\mathbf{X},0)$ and $\tilde{\mathbf{B}}^{inc}(\mathbf{X},0) + \tilde{\mathbf{B}}^r(\mathbf{X},0) = \tilde{\mathbf{B}}^t(\mathbf{X},0)$, where the superscripts *inc*, *r*, and *t* denote the incident, reflected, and transmitted field, respectively. Using Equation 7, these continuity conditions may be written as

$$\begin{pmatrix} \tilde{\mathbf{E}}^{inc}(\mathbf{X},0) \\ \tilde{\mathbf{B}}^{inc}(\mathbf{X},0) \end{pmatrix} + \begin{pmatrix} \tilde{\mathbf{E}}^r(\mathbf{X},0) \\ \tilde{\mathbf{B}}^r(\mathbf{X},0) \end{pmatrix} = \begin{pmatrix} \tilde{\mathbf{E}}^t(\mathbf{X},0) \\ \tilde{\mathbf{B}}^t(\mathbf{X},0) \end{pmatrix} = \begin{pmatrix} \tilde{\mathbf{E}}^t(\mathbf{X},0) \\ \mathbf{S}_{21}(\mathbf{X})\left[\mathbf{S}_{11}(\mathbf{X})\right]^{-1}\tilde{\mathbf{E}}^t(\mathbf{X},0) \end{pmatrix} \tag{8}$$

The incident fields represent the Gaussian incident beam. To solve for the transmitted $\tilde{\mathbf{E}}^t$ and reflected $\tilde{\mathbf{E}}^r$ electric fields, we need a relationship between $\tilde{\mathbf{E}}^r$ and $\tilde{\mathbf{B}}^r$ and since these latter fields are in the homogeneous superstrate region, we can write these fields as Fourier expansions

$$\tilde{\mathbf{E}}^r(\mathbf{X},z)=\mathbf{F}(\mathbf{X},\mathbf{K})\tilde{\mathbf{E}}^r(\mathbf{K},z) \quad \text{and} \quad \tilde{\mathbf{B}}^r(\mathbf{X},z)=\mathbf{F}(\mathbf{X},\mathbf{K})\tilde{\mathbf{B}}^r(\mathbf{K},z) \tag{9}$$

These Fourier expansions are written in matrix form where the square matrix $\mathbf{F}(\mathbf{X},\mathbf{K})$ is a Fourier transform operator. The $\mathbf{K}$ denotes the set of wave vectors in Fourier space analogous to the set of x coordinates $\mathbf{X}$ in real space. In Fourier space and with Maxwell's equations, we can further relate $\tilde{\mathbf{E}}^r(\mathbf{K},0)$ and $\tilde{\mathbf{B}}^r(\mathbf{K},0)$ by

$$\tilde{\mathbf{B}}^r(\mathbf{K},0)=\mathbf{Z}(\mathbf{K})\tilde{\mathbf{E}}^r(\mathbf{K},0) \tag{10}$$

where $\mathbf{Z}(\mathbf{K})$ is a square matrix defined elsewhere (References 1 and 3). Using Equations 9 and 10 in Equation 8 yields

$$\begin{pmatrix} \mathbf{I} & -\mathbf{I} \\ \mathbf{S}_{21}\mathbf{S}_{11}^{-1} & -\mathbf{F}\mathbf{Z}\mathbf{F}^{-1} \end{pmatrix}\begin{pmatrix} \tilde{\mathbf{E}}^t(\mathbf{X},0) \\ \tilde{\mathbf{E}}^r(\mathbf{X},0) \end{pmatrix}=\begin{pmatrix} \tilde{\mathbf{E}}^{inc}(\mathbf{X},0) \\ \tilde{\mathbf{B}}^{inc}(\mathbf{X},0) \end{pmatrix} \tag{11}$$

where $\mathbf{I}$ is the identity matrix. Equation 11 can be solved for $\tilde{\mathbf{E}}^t(\mathbf{X},0)$ and then, from Equation 5 we find that $\mathbf{C}_+=\mathbf{S}_{11}^{-1}\tilde{\mathbf{E}}^t(\mathbf{X},0)$ that further yields the transmitted electric field for depths $z \le 0$ as

$$\tilde{\mathbf{E}}^t(\mathbf{X},z)=\mathbf{S}_{11}\mathbf{e}^{\lambda z}\mathbf{S}_{11}^{-1}\tilde{\mathbf{E}}^t(\mathbf{X},0) \tag{12}$$

This is our primary theoretical result from which we obtain numerical results below.

NUMERICAL RESULTS

The numerical results were obtained with the following physical parameters: ω/c = 1.5 inverse micrometers (wavelength = 4.19 micrometers), σ = 3.0 micrometers, d = 3.0 micrometers and L = 30 micrometers. The number of digitized points was $n_x = 1001$,

which yields Δx = 0.03 micrometers. The permittivity values are $\varepsilon_1 = (-16,0)$ and $\varepsilon_2 = (2.25,0)$.

In Figure 3, we illustrate the existence of guided wave modes by looking at the inverse square of the dispersion relation for both p- and s-polarization. The dispersion relations are obtained for the z < 0 region by matching boundary conditions and finding the electromagnetic field solutions within this region. The peaks indicate the wave numbers k_z which satisfy the dispersion relation for the fixed ω and therefore represent wave numbers associated with guided mode solutions. For frequency ω/c = 1.5 inverse micrometers and d = 3.0 micrometers, we see that there are three p-polarization mode peaks and two s-polarization mode peaks. These peaks indicate guided-mode solutions, which propagate in the z direction along the guided wave structure described in this work. Figures 4 through 6 describe coupling of the incident beam into these guided modes.

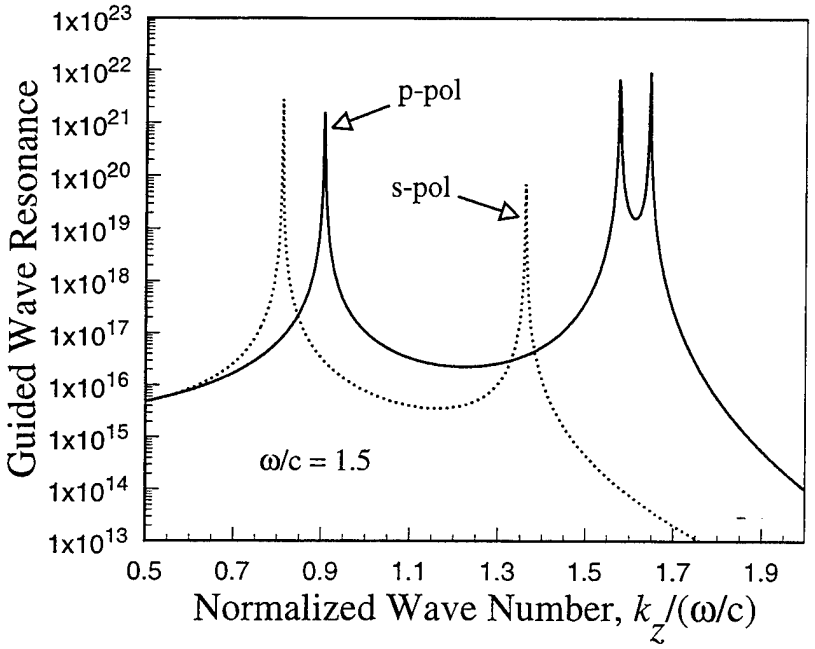

FIGURE 3. Guided-Wave Resonance Versus Wave Number k_z at Fixed Frequency ω. This graph indicates three p-pol (magnetic vector parallel to guide boundaries) mode solutions and two s-pol (electric vector parallel to guide boundaries) mode solutions.

For p-polarization, Figure 4 shows the intensity of the incident field (at z = 0) and transmitted field (Equation 12 at z = 0 and $z = -500\lambda$). It is seen that there is significant coupling of the incident beam into the planar waveguide where the reflectance and transmittance is 0.335 and 0.665, respectively.

In Figure 4, it is seen that there are some interesting observations about the three p-pol modes shown in Figure 3. First, the mode indicated at $k_z/(\omega/c) = 0.9$ ($k_z = 1.35$ inverse microns) is associated with a guided mode, which has peak intensity around x = 0 and minimum intensity at the guide boundaries. This intensity peak is seen as the slight negative curvature (about x = 0) of the two guided-mode curves. Also, this mode is propagating (non-evanescent) in both the x and z directions. The other two p-pol peaks in Figure 3 are centered about $k_z/(\omega/c) \approx 1.62$. This indicates that they are associated with coupled surface waves that are evanescent relative to the metal-dielectric waveguide boundaries. Thus, these modes are evanescent in the x direction and propagating in the z direction. To see this, we note that a surface plasmon that propagates along a metal-dielectric interface has dispersion relation $k_{sp}/(\omega/c) = \sqrt{\varepsilon_1\varepsilon_2/(\varepsilon_1+\varepsilon_2)}$ and, for the permittivity parameters used here, this yields $k_{sp}/(\omega/c) = 1.618$. The two p-pol peaks seen in Figure 3 are split about this value with the splitting due to coupling between the surface waves at each interface. Finally, we note that since these modes are evanescent, their intensity is a maximum at the guide interfaces.

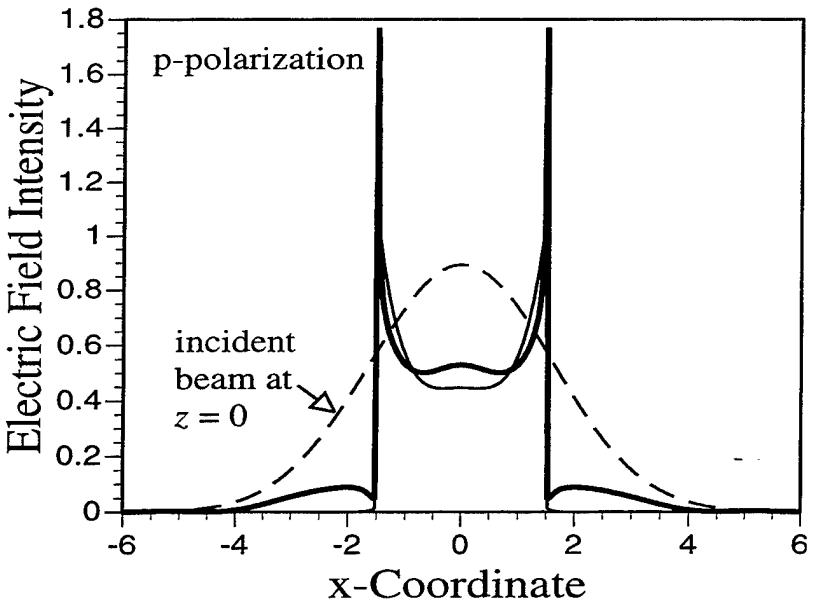

FIGURE 4. Electric Field Intensity Versus x Coordinate For P-Polarization and ω/c = 1.5 Inverse Microns. For reference, the $z = 0$ Gaussian beam envelope is indicated (dash line). The remaining two intensity curves are for the transmitted field (Eq. (12)) at $z = 0$ (thick line) and $z = -500\lambda$. (thin line). The planar waveguide boundaries are at $x = \pm$ 1.5 micrometers.

For p-polarization, there is another surface mode, not indicated in Figure 3, with which there is coupling: the surface plasmon at the z = 0 metal-vacuum interface. This surface plasma mode is confined to the metal-vacuum interface (evanescent in the z direction) and

propagates in the x direction. Coupling can occur between the incident and metal-vacuum surface plasmon field because of the discontinuity of the dielectric waveguide channel. This surface plasmon, with wave number k_{sp}, has dispersion relation $k_{sp}/(\omega/c) = \sqrt{\varepsilon_2/(\varepsilon_2+1)}$ = 1.0324 for $\varepsilon_2 = (-16,0)$. This surface plasmon coupling is evident in Fig.5 which shows the Fourier spectrum of the electric field at z = 0 and -500λ. Figure 5 is a plot of the Fourier transform of $\tilde{\mathbf{E}}^t(\mathbf{X},z)$, which is the Fourier spectrum $\tilde{\mathbf{E}}^t(k_x,z)$, versus $k_x/(\omega/c)$. In Figure 5, most Fourier components are concentrated about $k_x = 0$. However, for the thick curve (z = 0) there are two peaks about $k_x/(\omega/c) \approx \pm 1.1$ and we interpret these as wave numbers associated with the surface plasmon. For the dot curve ($z = -500\lambda$), we see there are no similar peaks.

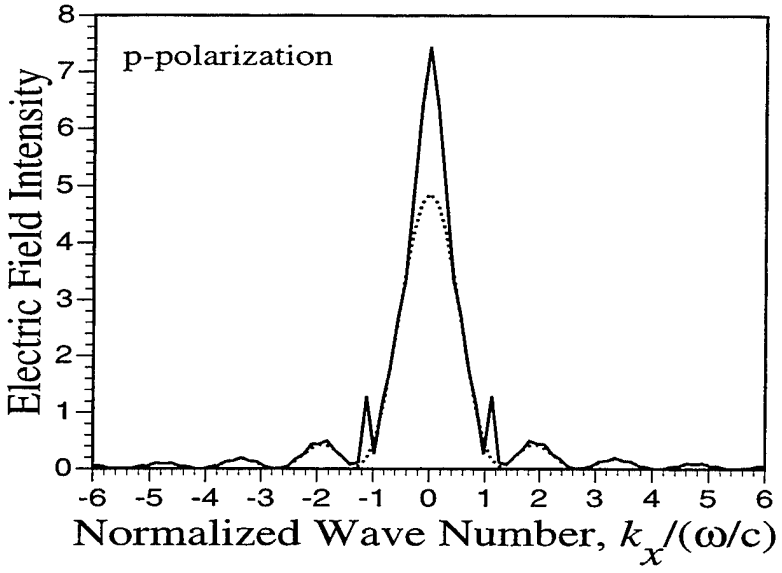

FIGURE 5. Electric Field Intensity Versus Wave Number k_x for ω/c = 1.5 Inverse Microns and p-Polarization. The solid and dot curves are for z = 0 and -500λ, respectively. The solid curve shows two sharp peaks centered about $1<\pm k_x<1.2$ which indicate coupling with surface plasmons which propagate along the x direction. The remaining Fourier spectrum is associated with propagation of guided waves in the planar waveguide along the z direction.

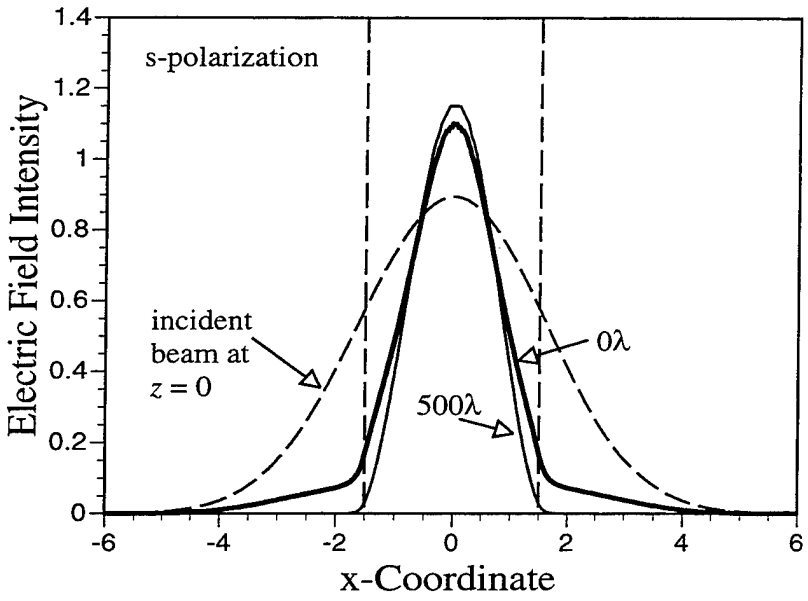

FIGURE 6. Electric Field Intensity Versus x Coordinate for s-Polarization and $\omega/c = 1.5$ Inverse Microns. For reference, the $z = 0$ Gaussian beam envelope is indicated. The remaining two intensity curves are for the transmitted field (Equation 12) at $z = 0$ (thick line) and $z = -500\lambda$ (thin line). The planar waveguide boundaries are at $x = \pm 1.5$ micrometers as shown by the vertical dash lines.

The result for s-polarization is shown in Figure 6. Again, the Gaussian beam at $z = 0$ is shown for reference. The vertical dashed lines indicate the boundaries of the waveguide channel where $|x| \leq 1.5$ micrometers. The thin and thick curves are the electric field intensity at $z = 0$ and $z = -500\lambda$, respectively. Again, it is seen that there is significant coupling into the guided wave channel where the reflectance and transmittance are 0.282 and 0.718, respectively. Note that for this polarization, there are no evanescent surface modes and this solution propagates in both the x and z directions. The electric field intensity is peaked about $x = 0$.

CONCLUSIONS

We have described a method of calculating the reflected and transmitted fields associated with a Gaussian intensity beam incident endwise upon a planar waveguide structure. The numerical results indicate that a majority of incident energy can be coupled into the planar structure. The results account for guided modes which propagate down the planar guide and for surface modes associated with the metal-vacuum interface.

REFERENCES

1. J. M. Elson and P. Tran. "Dispersion and Diffraction in Photonic Media: A Different Modal Expansion For the **R**-Matrix Propagation Technique," *J. Opt. Soc. Am.,* Vol. A12 (1995), pp. 1765-1771.

2. Naval Air Warfare Center Weapons Division. *A Real Space, Modal Expansion Method With the **R**-Matrix Propagator to Calculate Grating Diffraction*, by J. M. Elson and P. Tran. China Lake, Calif., NAWCWPNS, September 1996. (NAWCWPNS TP 8318, publication UNCLASSIFIED.)

3. J. M. Elson and P. Tran. "Coupled Mode Calculation With the **R**-Matrix Propagator For the Dispersion of Surface Waves on a Truncated Photonic Crystal," *Phys. Rev.*, Vol. B54 (1996), pp. 1711-1715.

4. J. M. Elson and P. Tran. "Band Structure and Transmission of Photonic Media: A Real-Space Finite-Difference Calculation With the **R**-Matrix Propagator," in *Photonic Band Gap Materials,* Vol. 315, *NATO Advanced Study Institute Series E: Applied Sciences,* ed. by C. M. Soukoulis. Kluwer, Dordrecht, 1996. Pp. 341-354; see also J. M. Elson and P. Tran. *A Real-Space Numerical-Integration Approach to Calculate Diffraction From Gratings.* China Lake, Calif., NAWCWPNS, December 1996. (NAWCWPNS TP 8334, publication UNCLASSIFIED.)

5. A. R. McGurn, V. Malyshkin, J. M. Elson, and P. Tran. "Transverse Localization of Light in Two-Dimensional Random Structure," manuscript in progress.

INITIAL DISTRIBUTION

1 Commander in Chief, U. S. Pacific Fleet, Pearl Harbor (Code 325)
1 Naval War College, Newport
1 Headquarters, 497 IG/INT, Falls Church (OUWG Chairman)
2 Defense Technical Information Center, Fort Belvoir
1 Center or Naval Analyses, Alexandria, VA (Tehnical Library)

ON-SITE DISTRIBUTION

1 Code 400000D
1 Code 4B0000D
4 Code 4BL000D (3 plus Archives copy)
20 Code 4B1200D, Elson
1 Code 4B4000D, Chesnut